A Novel Finite-Control-Set Model Predictive Current Control for Five-Phase PM Motor With Continued Modulation

Wenxiang Zhao, *Senior Member, IEEE*, Tao Tao, Jihong Zhu, Huajun Tan, and Yuxuan Du

***Abstract*—The conventional five-phase finite-control-set model predictive control (FCS-MPC) suffers from heavy computational burden. Meanwhile, the control set with finite vectors inevitably leads to deteriorated operation performance. This article proposes a novel FCS model predictive current control (MPCC) with continued modulation. A cascaded optimization procedure is proposed, which includes main virtual voltage vector (VV) selection, determination of optimal combination of adjacent two VVs, and amplitude optimization. In this cascaded optimization procedure, the phase angle and the amplitude of the synthesized vector can be obtained in different steps. Also, there are two duty cycles calculated in different steps independently, which avoid overflow. By using this cascaded procedure, the continued modulation can be realized without using a modulator. Meanwhile, a vector selection method is introduced to reduce computational burden. This vector selection method avoids evaluation of all the candidate vectors without any negative effects. Moreover, the merits of conventional FCS-MPCC can be preserved. The experimental results verify the effectiveness and superiority of the proposed FCS-MPCC method.**

***Index Terms*—Computational time, current harmonics, five-phase motor, model predictive control (MPC), permanent-magnet motor, virtual voltage vector (VV).**

I. Introduction

Owing to the increasing computational power of modern microprocessors, the implementation of finite-control-set model predictive control (FCS-MPC) in standard control hardware platform has become a reality [1]–[5]. The FCS-MPC has been the main competitor to field-oriented control and direct torque control due to intuitive concept [6], fast dynamic response [7], and easy inclusion of constraints [8].

Manuscript received July 21, 2019; revised October 7, 2019; accepted November 11, 2019. Date of publication November 16, 2019; date of current version March 13, 2020. This work was supported in part by the National Natural Science Foundation of China under Grant 51777090, in part by the Key Research and Development Program of Jiangsu Province under Grant BE2018107, in part by the Six Talent Peaks Project of Jiangsu Province under Grant 2017-KTHY-011, and in part by the Priority Academic Program Development of Jiangsu Higher Education Institutions. Recommended for publication by Associate Editor H. Hoffman. *(Corresponding author: Wenxiang Zhao.)*

W. Zhao, T. Tao, H. Tan, and Y. Du are with the School of Electrical and Information Engineering, and also, with the Jiangsu Key Laboratory of Drive and Intelligent Control for Electric Vehicle, Jiangsu University, Zhenjiang 212013, China (e-mail: zwx@ujs.edu.cn; 15862935596@163.com; 1621323397@qq.com; dyxdoby@ujs.edu.cn).

J. Zhu is with the Department of Precision Instrument, Tsinghua University, Beijing 100084, China (e-mail: jhzhu@tsinghua.edu.cn).

Color versions of one or more of the figures in this article are available online at http://ieeexplore.ieee.org.

Digital Object Identifier 10.1109/TPEL.2019.2954285

The classic FCS-MPC comprises two steps: 1) to predict the control variable at the next interval; and 2) to evaluate all the candidate vectors through a cost function. Obviously, the exhausting process inevitably leads to heavy computational burden. In addition, the finite candidate vectors with fixed amplitude and phase angle deteriorate the operation performance. However, there are some special control considerations when the FCS-MPC is applied to multi-phase drives. First, the using of extended symmetrical component transformation leads to the introduction of fundamental space and harmonic space [10]–[13]. The harmonic currents inevitably result in a decrease in system efficiency. Hence, the suppression of harmonic currents is the exact challenge of the classic FCS-MPC for multiphase drives. Then, the exhausting process will be more time-consuming, because the voltage vectors increased exponentially with the increase of phase number [7], [11].

Some articles were published to address the aforementioned issues [14]–[21]. The virtual voltage vector (VV) synthesized from basic vectors are employed to restrain the harmonic components and to alleviate the computational burden. The VVs based finite-control-set model predictive current control (FCS-MPCC) was adopted for a five-phase motor [17] and a dual three-phase motor [18]. However, the fixed amplitude of the VVs deteriorates the operation performance. In order to change the amplitude of the VVs, the duty cycle modulation technology was adopted in [19]. However, the control object was a five-phase passive *R–L* load. Also, the vector selection and duty cycle calculations were evaluated separately. In [20], a model predictive torque control (MPTC) for an asymmetrical dual three-phase PM motor was introduced. This method took into account the suppression of harmonic currents and alleviated the computational burden simultaneously. However, the vector selection method can only be applied to the MPTC. The MPTC strategy for a five-phase PM synchronous motor with reduced harmonic currents and torque ripples was introduced in [21]. A quadratic evaluation method was introduced to relief the computational burden. However, this vector selection method cannot be applied by the MPCC. In [22], a constant switching frequency multiple vector MPCC for a five-phase PM motor with non-sinusoidal EMF was introduced. However, the voltage reference and the modulator were necessary, which increase the control complexity. In [23], a three-phase MPTC with extended control set was proposed to minimize the torque ripple. However, the drawback of discrete candidate vectors cannot be overcome.

The FCS-MPCs with continued modulation area were investigated in three-phase systems, which include active rectifier [24], rectifier [25], and grid-tied wind turbine system [26]. The general method is to obtain the optimal phase angle and to optimize the amplitude. Therefore, the adjacent two vectors and corresponding duty cycles are necessary. However, in [24] and [25], the two duty cycles were calculated simultaneously, which means the sum of the two duty cycles might exceed 1. In addition, for the five-phase system, the complexity of realizing continued modulation increased due to the harmonic subspace and computational burden.

In this article, a novel five-phase FCS-MPCC with continued modulation is proposed. The proposed method presents better steady-state performance without increasing the computational burden. The main contributions of this article are as follows.

1) A cascaded optimization procedure is introduced to realize continued modulation without using a modulator. In this cascaded optimization procedure, the amplitude and phase angle of the synthesized vector can be determined by defining two cost functions and adopting the duty cycle modulation technology twice.
2) A vector selection method with reduced computational burden is introduced. This method eliminates repeated vector combinations. Also, the optimal VVs can be selected accurately.
3) The experimental evaluations of the proposed method with the existing methods are conducted.

The rest of the article is organized as follows. In Section II, the VVs based FCS-MPCC is introduced. In Section III, the duty cycle modulation technology is introduced, which can be adopted to extend the modulation area. A novel finite control is proposed in Section IV. Section V provides experimental results to show and discuss the performance of the proposed method. Finally, Section VI concludes this article.

II. VVs Based FCS-MPCC

The motor is supplied by a two-level five-phase voltage source inverter, which has $2^5 = 32$ switching states. Each switching state combination corresponds to a voltage space vector in the α–β and *x*–*y* spaces. Fig. 1 shows the voltage vectors in the α–β and *x*–*y* spaces. The vectors can be classified into three groups with different amplitudes, from innermost to outmost: small, medium, and large. It should be noted that the large vectors in the α–β space project in the *x*–*y* space as the small vectors and vice versa.

According to the vector space decomposition approach, the α–β space is responsible for torque production. The harmonic currents in the *x*–*y* space deteriorate the operation performance and reduce the system efficiency. Hence, it is necessary to suppress the harmonic currents.

The VV synthesized from two basic vectors aim to reduce the harmonic component for five-phase FCS-MPCC was introduced in [17]. The synthetic principle can be expressed as follows:

$$\mathrm{VV}_i(u_M, u_L) = 0.382 \cdot u_M + 0.618 \cdot u_L \tag{1}$$

where u_M and u_L are the two basic vectors in medium and large groups, respectively. The 10 VVs and 2 null vectors depicted in Fig. 2 can be employed as the control set. The VV which minimizes a predefined cost function can be selected to generate the drive signal.

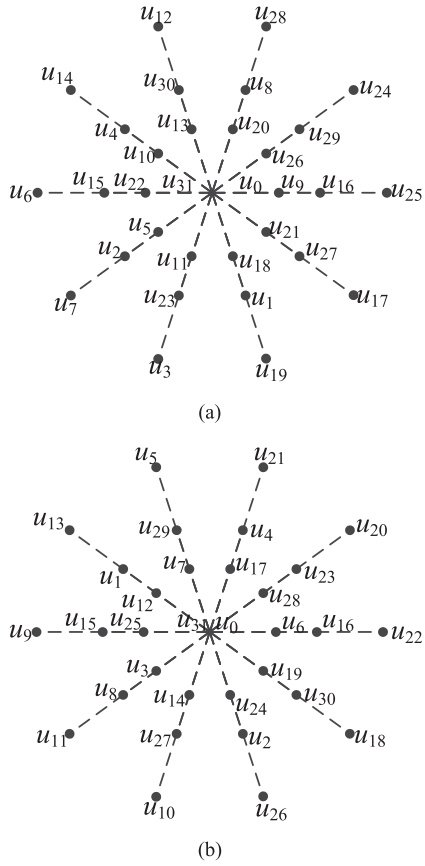

Fig. 1. Voltage space vectors of five-phase drive. (a) α–β space. (b) *x*–*y* space.

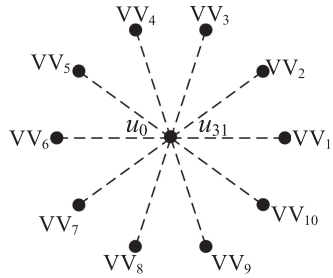

Fig. 2. Projections of VVs.

According to the principle of classic FCS-MPCC, the predicted currents at the $(k+1)$th instant can be expressed as follows:

$$i_s(k+1) = i_s(k) + \frac{T_s}{L_s}(u_s - r_s i_s(k)) + e_{dq}$$
$$\text{s.t. } u_s \in \{u_0, \mathrm{VV}_{1\_dq}, \mathrm{VV}_{2\_dq} \ldots\ldots, u_{31}\} \tag{2}$$

where

$$i_s = [i_d \;\; i_q]^T \quad L_s = [L_d \;\; L_q]^T$$
$$e_{dq} = [\omega L_q i_q \quad -\omega(L_d i_d + \psi_f)]^T$$

and r_s is the stator resistance, L_d and L_q are the *d–q* axis inductances, respectively, i_d and i_q are the *d–q* axis currents, respectively, ω is the angular velocity, T_s is the sampling period, and ψ_f is the PM flux linkage.

The rotational transformation (3) can be used to transform α–β space components into the synchronously rotating reference frame

$$u_s = \begin{bmatrix} \cos(\theta_r) & \sin(\theta_r) \\ -\sin(\theta_r) & \cos(\theta_r) \end{bmatrix} \begin{bmatrix} \text{real}(\text{VV}_i) \\ \text{imag}(\text{VV}_i) \end{bmatrix} \tag{3}$$

where θ_r is the rotor position.

Generally, the VVs based FCS-MPCC is effective to restrain the harmonic components and reduce the computational burden simultaneously. However, the modulation area of the VVs based FCS-MPCC is restricted to 10 VVs and 2 null vectors. The discontinued modulation area leads to deteriorated operation performance.

III. Duty Cycle Modulation Technology

As mentioned above, the selected vector is applied to the inverter for the whole control period. The finite and discontinued vectors are the main reason for deteriorated operation performance. In order to extend the modulation area, the duty cycle modulation technology is adopted.

In this article, the deadbeat principle of the *d–q* space currents is used to calculate the optimal duty cycle. According to this principle, the *d–q* space currents at the $(k+1)$th instant should reach its reference values. This can be expressed as follows:

$$i_s(k+1) = i_s(k) + s_i T_{\text{vv}_i} + s_j (T_s - T_{\text{vv}_i}) = i_s^* \tag{4}$$

where

$$s_i = \left.\frac{di_s}{dt}\right|_{u_s = \text{VV}_i}$$

$$s_j = \left.\frac{di_s}{dt}\right|_{u_s = T_s - T_{\text{vv}_i}}$$

and T_{vv_i} is the execution time of VV_i. i_s^* is the reference current of the *d–q* space. In this article, the $i_s^* = 0$ strategy is adopted. The output of the speed regulator is the reference current of the *q*-axis.

Equation (4) is a function of T_{vv_i}. The optimal execution time can be calculated by solving

$$\frac{\partial \text{normal}(i_s^* - i_s(k+1))^2}{\partial T_{\text{vv}_i}} = 0. \tag{5}$$

The duty cycle and execution time of VV_i can be obtained as follows:

$$d(i) = \frac{dot((i_s^* - i_s(k) - s_j T_s), (s_i - s_j))}{T_s \times (s_i - s_j)^2} \tag{6}$$

$$T_{\text{VV}_i} = d(i) \times T_s. \tag{7}$$

By adopting the duty cycle modulation technology, the modulation area can be extended from two discontinued VVs to a line between the two VVs. It should be noted that exchanging the sequence order of vector combination does not affect the operation performance [27]. This merit can be used to alleviate the computational burden.

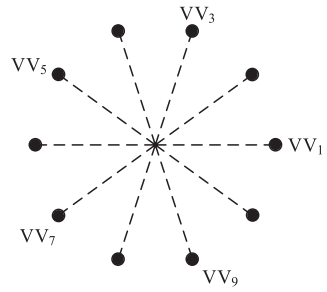

Fig. 3. Projection of main vectors.

TABLE I
Combination of Adjacent VVs

Main VV_i	Auxiliary VV_j	
VV_1	VV_2	VV_{10}
VV_3	VV_4	VV_2
VV_5	VV_6	VV_4
VV_7	VV_8	VV_6
VV_9	VV_{10}	VV_8

IV. Proposed Control

In this section, a cascaded optimization procedure is introduced to realize continued modulation. Also, a vector selection method is introduced to reduce the computational burden. This optimization procedure includes the following three steps.

Step 1: Determination of the main VV.
Step 2: Determination of phase angle.
Step 3: Amplitude optimization.

A. Determination of Phase Angle

Step 1: In *Step 1*, a simplified control set is employed, as shown in Fig. 3. The VVs in Fig. 3 are named as the main VV in this article.

The principle of classic FCS-MPCC is adopted to evaluate the simplified control set. In this situation, the predictive model and the control set can be expressed as follows:

$$\begin{aligned} &i_s(k+1) = i_s(k) + \frac{T_s}{L_s}(u_s - r_s i_s(k) + e_{dq}) \\ &\text{s.t. } u_s \in \{\text{VV}_{1\_dq}, \text{VV}_{3\_dq}, \text{VV}_{5\_dq}, \text{VV}_{7\_dq}, \text{VV}_{9\_dq}\}. \end{aligned} \tag{8}$$

The first cost function is defined to determine the optimal main VV, which can be expressed as follows:

$$\text{cost function } 1 = \text{normal}(i_s^* - i_s(k+1))^2 \tag{9}$$

Step 2: After the main VV is determined, the adjacent two VVs of the main VV will be evaluated. The adjacent two VVs are named as auxiliary VV. The combinations of main VVs and corresponding auxiliary VVs are listed in Table I.

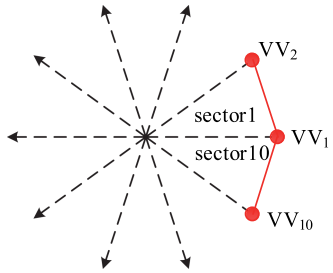

Fig. 4. Projection of adjacent VVs through duty cycle modulation.

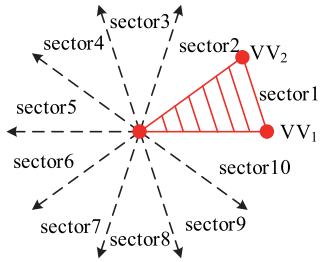

Fig. 5. Modulation area of sector1.

Assuming the optimal main VV is VV_1, the duty cycles of the two auxiliary VVs can be calculated as follows:

$$d_1(j) = \frac{\mathrm{dot}((i_s^* - i_s(k) - s_{\mathrm{VV}_1}T_s), (s_{\mathrm{VV}_j} - s_{\mathrm{VV}_1}))}{T_s \times (s_{\mathrm{VV}_j} - s_{\mathrm{VV}_1})^2} \quad (10)$$

where

$$s_{\mathrm{VV}_1} = \left.\frac{di_s}{dt}\right|_{u_s=\mathrm{VV}_1}$$

$$s_{\mathrm{VV}_j} = \left.\frac{di_s}{dt}\right|_{u_s=\mathrm{VV}_j}.$$

The two synthetic vectors can be expressed as follows:

$$u_{adj\_\alpha\beta}(j) = d_1(j) \times \mathrm{VV}_j + (1 - d_1(j)) \times \mathrm{VV}_1. \quad (11)$$

The two synthetic vectors in (11) are evaluated by adopting the principle of classic FCS-MPCC again. In this situation, the predictive current model and control set can be expressed as follows:

$$i_s(k+1) = i_s(k) + \frac{T_s}{L_s}(u_s - r_s i_s(k) + e_{dq})$$

$$\text{s.t. } u_s \in \{u_{adj\_dq}(2), u_{adj\_dq}(10)\}. \quad (12)$$

The second cost function is defined to determine the optimal auxiliary VV and corresponding duty cycle, which can be expressed as follows:

$$\text{cost function } 2 = \mathrm{normal}(i_s^* - i_s(k+1))^2. \quad (13)$$

It should be noted that the cost function 1 and cost function 2 have the same form. The difference is the control set.

In one sampling period, the optimal synthetic vector is located at the line between the main VV and auxiliary VV, as shown in Fig. 4.

Generally, *Step 1* and *Step 2* are used to determine the phase angle of the optimal synthetic vector. Actually, in one control period, the phase angle can be determined in two ways. In the first way, VV_1 is selected from *Step 1* and VV_2 is selected from *Step 2*. In the second way, VV_2 is selected from *Step 1* and VV_1 is selected from *Step 2* (this possibility is not involved in Table I). In other words, if all the ten VVs are evaluated in *Step 1*, the other nine VVs are considered in *Step 2*, the number of exhausting processes is large, which will bring huge computational burden. Moreover, the combinations of nonadjacent VVs are meaningless. By using this vector selection method, the computational burden is reduced, because the repeated and meaningless combinations can be abandoned. Also, even though there are some vectors will not be evaluated in one control period, the optimal vector can be selected accurately. This is because the combinations in Table I have considered all the sectors.

By adopting the duty cycle modulation technology, the modulation area can be extended from 12 discrete candidate vectors to a regular decagon. It should be noted that the optimal auxiliary VV and corresponding duty cycle can be evaluated simultaneously through cost function 2. This means the phase angle can be determined.

B. Amplitude Optimization

Step 3: A main drawback of the conventional FCS-MPCC is the fixed amplitude of the candidate vectors. This is because, in conventional FCS-MPCC, the null vectors are evaluated independently. Actually, the null vectors can be used to change the amplitude of active vectors rather than applied to the inverter directly. It can be assumed that the VV_2 is the optimal auxiliary VV. The duty cycle of the synthetic vector can be expressed as follows:

$$d_2 = \frac{dot((i_s^* - i_s(k) - s_0T_s), (s_{adj} - s_0))}{T_s \times (s_{adj} - s_0)^2} \quad (14)$$

where

$$s_{adj} = \left.\frac{di_s}{dt}\right|_{u_s=u_{adj\_dq(2)}}$$

$$s_0 = \left.\frac{di_s}{dt}\right|_{u_s=u_0 \text{ or } u_{31}}.$$

The synthetic vector of adjacent two VVs with optimal amplitude can be expressed as follows:

$$u_{opt\_\alpha\beta} = d_2 \times u_{adj\_\alpha\beta}(2) + \frac{(1-d_2)}{2} \times (u_0 + u_{31}). \quad (15)$$

By inserting the null vectors, the continued modulation area can be realized, as shown in Fig. 5.

In this step, there is no exhausting process, and only the two null vectors are used to optimize the amplitude of adjacent synthetic voltage vectors. The d_2 can be obtained according to the current work condition.

TABLE II
DUTY CYCLES OF EACH SECTOR

Sector	d_A	d_B	d_C	d_D	d_E
1	$(1+d_2)/2$	$(1+0.24d_2+0.76d_1d_2)/2$	$(1-d_2+0.76d_1d_2)/2$	$(1-d_2)/2$	$(1+0.24d_2-0.47d_1d_2)/2$
2	$(1+0.24d_2+0.76d_1d_2)/2$	$(1+d_2)/2$	$(1+0.24d_2-0.47d_1d_2)/2$	$(1-d_2)/2$	$(1-d_2+0.76d_1d_2)/2$
3	$(1+0.24d_2-0.47d_1d_2)/2$	$(1+d_2)/2$	$(1+0.24d_2+0.76d_1d_2)/2$	$(1-d_2+0.76d_1d_2)/2$	$(1-d_2)/2$
4	$(1-d_2+0.76d_1d_2)/2$	$(1+0.24d_2+0.76d_1d_2)/2$	$(1+d_2)/2$	$(1+0.24d_2-0.47d_1d_2)/2$	$(1-d_2)/2$
5	$(1-d_2)/2$	$(1+0.24d_2-0.47d_1d_2)/2$	$(1+d_2)/2$	$(1+0.24d_2+0.76d_1d_2)/2$	$(1-d_2+0.76d_1d_2)/2$
6	$(1-d_2)/2$	$(1-d_2+0.76d_1d_2)/2$	$(1+0.24d_2+0.76d_1d_2)/2$	$(1+d_2)/2$	$(1+0.24d_2-0.47d_1d_2)/2$
7	$(1-d_2+0.76d_1d_2)/2$	$(1-d_2)/2$	$(1+0.24d_2-0.47d_1d_2)/2$	$(1+d_2)/2$	$(1+0.24d_2+0.76d_1d_2)/2$
8	$(1+0.24d_2-0.47d_1d_2)/2$	$(1-d_2)/2$	$(1-d_2+0.76d_1d_2)/2$	$(1+0.24d_2+0.76d_1d_2)/2$	$(1+d_2)/2$
9	$(1+0.24d_2+0.76d_1d_2)/2$	$(1-d_2+0.76d_1d_2)/2$	$(1-d_2)/2$	$(1+0.24d_2-0.47d_1d_2)/2$	$(1+d_2)/2$
10	$(1+d_2)/2$	$(1+0.24d_2-0.47d_1d_2)/2$	$(1-d_2)/2$	$(1-d_2+0.76d_1d_2)/2$	$(1+0.24d_2+0.76d_1d_2)/2$

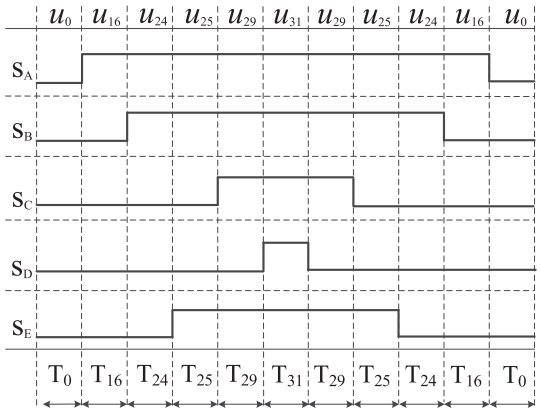

Fig. 6. Switching patterns of sector 1.

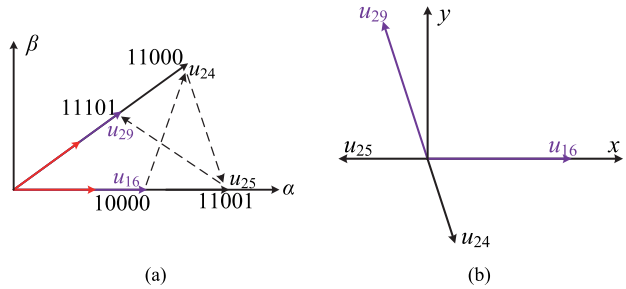

Fig. 7. Projections of switching sequencer in sector 1. (a) α–β space. (b) x–y space.

C. Pulse Generation

For the FCS-MPCC, the inverter is directly driven by applying the optimal switching state. It is necessary to discuss the switching patterns of the proposed method. In this work, a standard switching sequence is generated, which is easy to implement by the digit control system. Taking sector 1 as an illustration, the switching patterns are presented in Fig. 6. The actual applied voltage vector sequence is u_0–u_{16}–u_{24}–u_{25}–u_{29}–u_{31}–u_{29}–u_{25}–u_{24}–u_{16}–u_0 where

$$T_0 = \frac{(1-d_2)\times T_s}{4}$$

$$T_{31} = \frac{(1-d_2)\times T_s}{2}$$

$$T_{16} = \frac{d_2(1-d_1)\times 0.382\times T_s}{2}$$

$$T_{25} = \frac{d_2(1-d_1)\times 0.618\times T_s}{2}$$

$$T_{29} = \frac{d_2 d_1\times 0.382\times T_s}{2}$$

$$T_{24} = \frac{d_2 d_1\times 0.618\times T_s}{2}.$$

It should be noted that the two duty cycles are calculated in two different steps, and d_2 is affected by d_1. The execution time of each leg is the interaction of d_1 and d_2. So, one merit of this cascaded optimization procedure is that it can avoid the overflow. Fig. 7(a) depicts the voltage vector sequence of sector 1 in the α–β space. According to Fig. 7(b), it can be seen that even though the duty cycles of the two steps vary in different sampling periods, the harmonic-free can be preserved. This is because the adjacent two VVs with fixed duration always exist. It should be noted that the switching patterns are the same as that of the five-phase SVPWM.

Similar results can be obtained for the rest sectors. The duty cycles of each sector are listed in Table II, which have standard switching patterns.

D. Overall Control Algorithm

The flowchart of the proposed FCS-MPCC is shown in Fig. 8. According to this block diagram, the basic principle of conventional FCS-MPCC is adopted twice. So, the proposed method has an intuitive concept. Also, the constraints such as the limited phase current can be added to the cost functions in the first and second steps [14]. This means that the merit of easy inclusion of constraints can be preserved. In addition, a good dynamic performance can be provided due to the high current control bandwidth [7]. Moreover, the inverter is directly driven by applying the duty cycles in Table II without calculating voltage references.

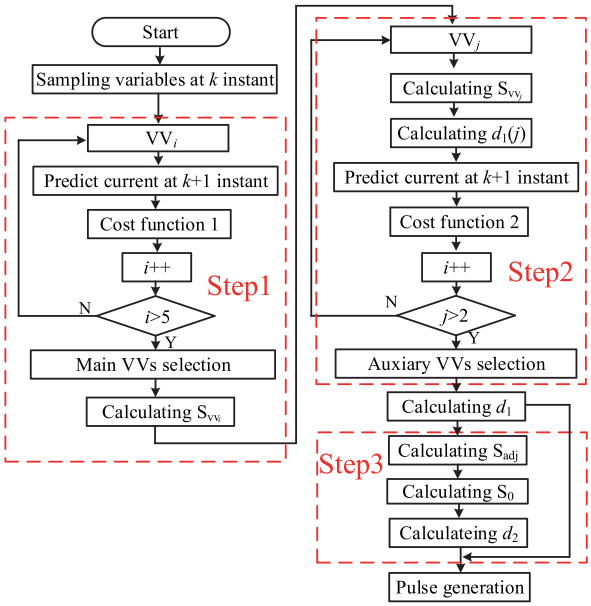

Fig. 8. Flowchart of the proposed FCS-MPCC.

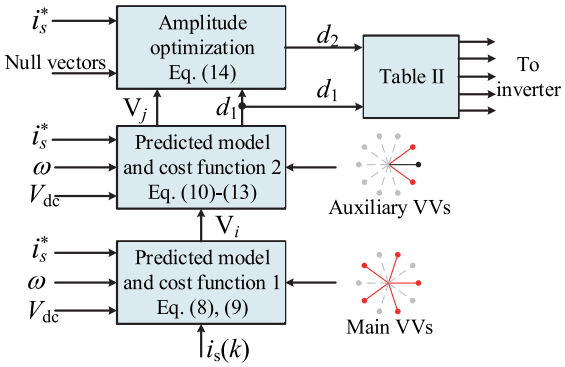

Fig. 9. Cascaded optimization procedure of the proposed method.

Fig. 9 shows the block diagram of the cascaded optimization procedure. Generally, the proposed FCS-MPCC provides the following advantages.

1) The computational burden can be reduced. This is because in *Step 1*, only five VVs are evaluated, and only two auxiliary VVs are considered in *Step 2*. The exhausting process can be reduced. Also, this vector selection method can be applied to FCS-MPTC.
2) The continued modulation can be obtained through a cascaded optimization procedure. The merits of conventional FCS-MPCC can be preserved.
3) The calculation process and implementation are simple. This is because the pre-synthetic VVs simplify the calculation process and the standard switching patterns are easy to generate.

V. Experimental Implementation

To verify the practicability and validity of the proposed FCS-MPCC, an experimental platform is established, which is shown in Fig. 10. A TMS320F28377 digital signal processor is employed for algorithm implementation. The sampling frequency is set to 20 kHz. A dc generator connecting a resistance is used as a load. The main parameters of the five-phase PM motor are listed in Table III.

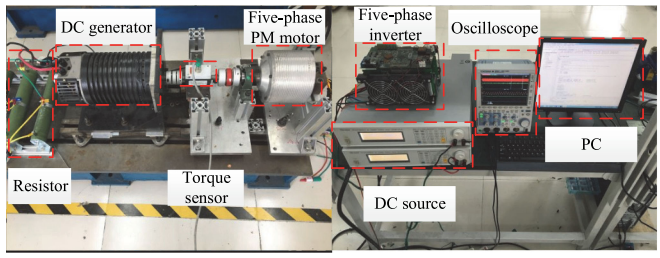

Fig. 10. Experimental platform.

TABLE III
Parameters of PM Motor

Parameter	Value	Unit
Rated power	1.2	kW
Rated speed	450	r/min
Number of pole pairs	31	
Number of stator slots	20	
PM flux-linkage	0.0248	Wb
d-q axis inductance	3.1	mH
Stator resistance	1.0	Ω

Two types of existing FCS-MPCC methods are compared to the proposed method. The FCS-MPCC introduced in [17] is carried out in this section. This method is named as VVs based FCS-MPCC. In addition, the duty cycle modulation technology introduced in Section III is adopted to optimize the amplitude of the VVs. This method is named as VVs based FCS-MPCC with optimal amplitude.

A. Steady-State Performance

Fig. 11(a)–(c) compare the steady-state performance of the three FCS-MPCCs mentioned above. The reference speed is set to 450 r/min and the load torque is set to 10 N·m.

It can be seen from Fig. 11(a) that the VVs based FCS-MPCC suffers from large harmonic currents and non-sinusoidal phase current. This is because the finite switching states inevitably lead to deteriorated operation performance. When the duty modulation technology is introduced, the amplitude of the VVs can be optimized, and the experimental result in Fig. 11(b) exhibits better performance in harmonic currents suppression. Also, the distortion of the phase current can be improved. This is because by using the duty cycle modulation technology, the modulation area can be extended. However, the modulation area of this method is restricted to ten lines.

Fig. 11(c) shows the steady-state performance of the proposed method. Compared with the two existing FCS-MPCC methods, the proposed method can achieve the lowest level of harmonic

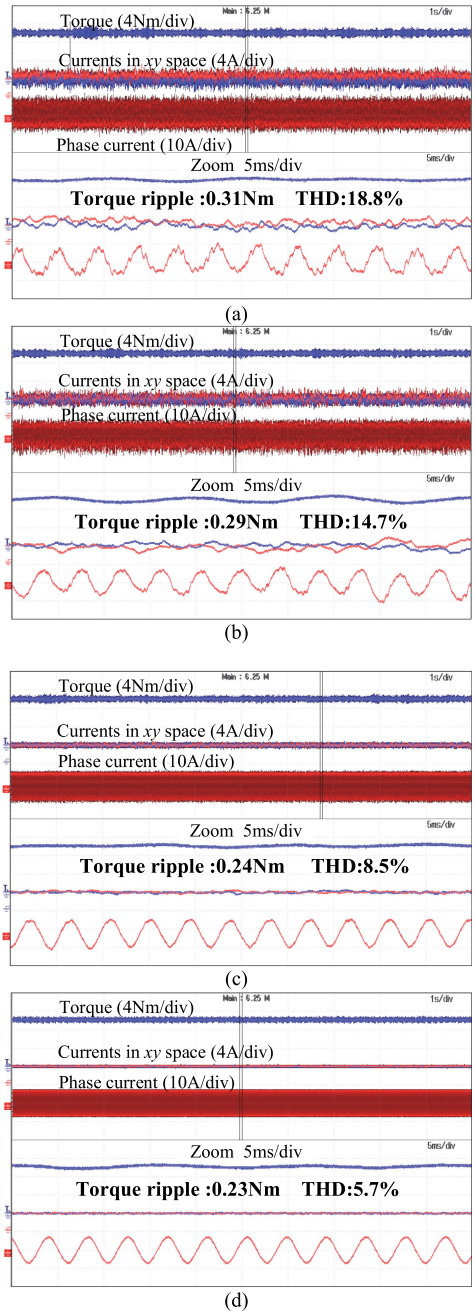

Fig. 11. Steady-state experimental results of different controls. (a) VVs based FCS-MPCC. (b) VVs based FCS-MPCC with optimal amplitude. (c) Proposed method. (d) PI-PWM method.

currents. Also, the phase current can achieve the lowest distortion. The reason is that the cascaded procedure employed in the proposed FCS-MPCC can realize continued modulation.

Fig. 11(d) shows the steady-state performance of the PI-PWM method. In this experiment, the proportional and integral coefficients of the four PI controllers are tuned elaborately. Compared with FCS-MPCC schemes, the best steady-state performance can be obtained.

According to Fig. 11, the deteriorated steady-state performance of conventional FCS-MPCC can be significantly improved by the proposed method. Compared with the PI-PWM method, the advantage of the proposed method is the easy tuning process. Especially in the application of multiphase drives, more current regulators and retuning processes are necessary for the PI-PWM method.

TABLE IV
EXECUTING TIME OF DIFFERENT FCS-MPCCS

	VVs based FCS-MPCC	VVs based FCS-MPCC with optimal amplitude	Proposed method
Executing time (*us*)	17.5	25.1	19.5

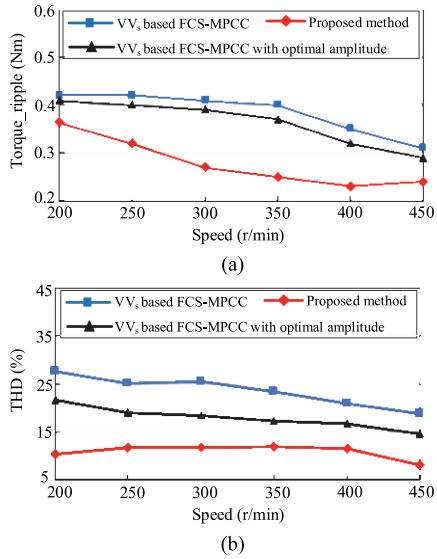

Fig. 12. Comparison of steady-state performances of different FCS-MPCC strategies under different speed conditions. (a) Torque ripple. (b) THD of phase current.

The execution time of different FCS-MPCCs is presented in Table IV. The execution time of the proposed method is slightly longer than the VVs based FCS-MPCC. This is because the cascaded procedure inevitably increases the amount of the code. Considering the improved performance, the increased extra time can be acceptable.

For a more convincing conclusion, the performances of two existing and one proposed FCS-MPCC methods are also compared under different work conditions. The values of torque ripple and THD of phase current are recorded. The experimental results of the three FCS-MPCC methods under different speed conditions are shown in Fig. 12. The load torque is set to 10 N·m. Fig. 13 depicts the experimental results of the three FCS-MPCC methods under different load torque conditions. The reference speed is set to 450 r/min. It is obvious from Figs. 12 and 13 that the proposed FCS-MPCC method can significantly reduce the THD of phase current and torque ripples under different work conditions.

B. Dynamic Performance

Fig. 14 shows the responses to external load disturbance of the proposed method. The reference speed is set to 450 r/min.

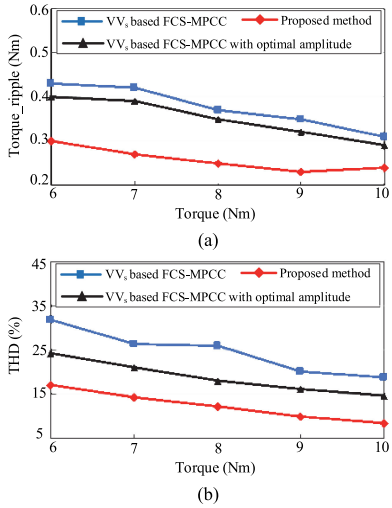

Fig. 13. Comparison of steady-state performances of different FCS-MPCC strategies under different load conditions. (a) Torque ripple. (b) THD of phase current.

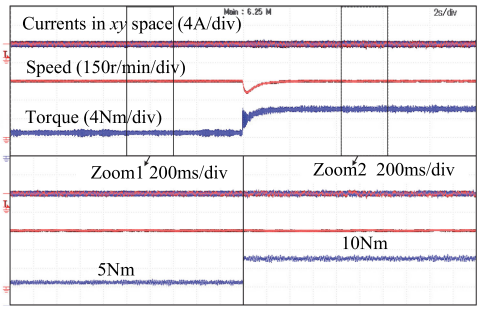

Fig. 14. Responses to external disturbance.

The load torque is changed from 5 to 10 N·m. It can be seen that the actual speed of the proposed method can get back to its original value quickly. This means that the proposed method has good robustness against external load disturbance. Meanwhile, the harmonic currents can be suppressed well under different load conditions.

Fig. 15 shows the dynamic performance of speed response, and the waveforms of harmonic currents, phase current, and actual speed are recorded. Fig. 15(a) shows the dynamic performance of the proposed method when the reference speed changes from 350 to 450 to 350 r/min with 10 N·m load. The dynamic performance of speed reversal is shown in Fig. 15(b). The speed command changes from 450 to −450 r/min with 10 N·m load. It can be seen that the proposed method can track the speed command very quickly. Meanwhile, the harmonic currents can be reduced well under different speed conditions. It should be noted that the load is a generator without controlling the voltage. So, the current amplitude increases at 450 r/min.

C. Robustness Performance Analysis

The calculation of the duty cycle relies on precise parameters of the PM motor. Therefore, it is necessary to conduct robustness performance analysis. The experimental results with

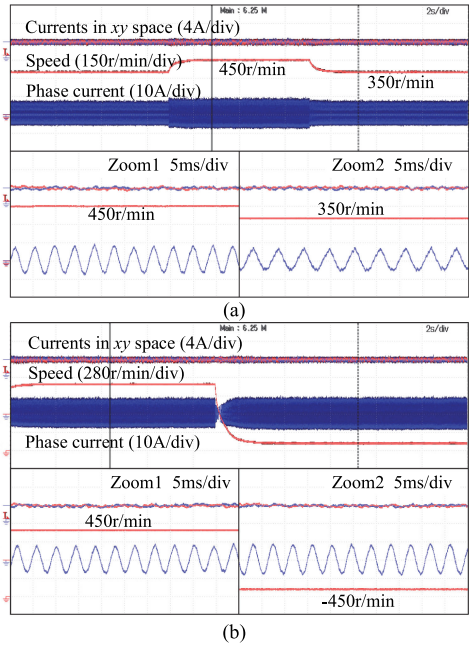

Fig. 15. Dynamic performance of speed response. (a) Reference speed: 350–450–350 r/min. (b) Reference speed: 450–450 r/min.

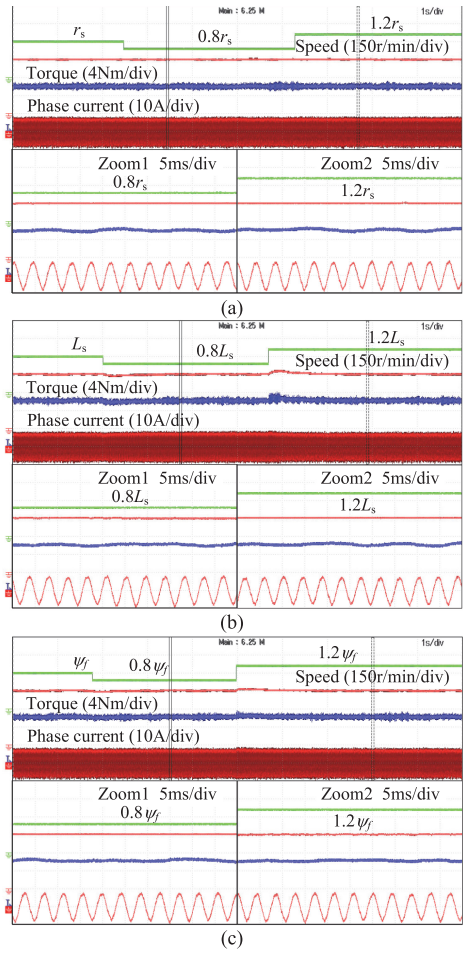

Fig. 16. Parameters sensitivity analysis. (a) Variation of stator resistance. (b) Variation of d–q axis inductance. (c) Variation of PM flux linkage.

inaccurate parameters are shown in Fig. 16. The experiments start with accuracy parameters, at a time instant, the parameters (stator resistance, *d-q* axis inductance and PM flux linkage) decreased to 80% of the accurate value. After a few seconds, the parameters increased to 120% of accurate value. It can be seen from Fig. 16(a) and (c) the performance is not affected by the mismatch of stator resistance and PM flux linkage. The experimental result of *d–q* axis inductance with inaccurate parameters is depicted in Fig. 16(b). At the instance of the change of *d–q* axis inductances, the actual speed is influenced, and return to reference value quickly. Thus, it can be concluded that the proposed strategy relatively minimizes the influence of parameter variations.

VI. Conclusion

This article has proposed a novel FCS-MPCC algorithm for a five-phase motor drive. Compared with the existing methods, the proposed method introduces a cascaded optimization procedure, which can realize continued modulation. Meanwhile, the reduction of computational burden and harmonic currents is taken into consideration. The proposed FCS-MPCC is easy because the VVs synthesized from two basic vectors can be considered as a whole. In addition, standard switching patterns can be generated, which is easy to implement. The steady-state performance under different work conditions is recorded. The experimental results show that the proposed FCS-MPCC can significantly improve the steady-state performance. Moreover, the proposed FCS-MPCC has good dynamic performance, and the harmonic currents of the proposed FCS-MPCC can be suppressed well even in the transition process. More importantly, the cascaded optimization process can be utilized to MPTC.

References

[1] W. Huang, W. Hua, F. Yin, F. Yu, and J. Qi, "Model predictive thrust force control of a linear flux-switching permanent magnet machine with voltage vectors selection and synthesis," *IEEE Trans. Ind. Electron.*, vol. 66, no. 6, pp. 4958–4967, Jun. 2019.

[2] X. Zhang, B. Wang, U. Manandhar, H. B. Gooi, and G. Foo, "A model predictive current controlled didirectional three-level DC/DC converter for hybrid energy storage system in DC microgrids," *IEEE Trans. Power Electron.*, vol. 34, no. 5, pp. 4025–4030, May 2019.

[3] G. A. Papafotiou, G. D. Demetriades, and V. G. Agelidis, "Technology readiness assessment of model predictive control in medium- and high voltage power electronics," *IEEE Trans. Ind. Electron.*, vol. 63, no. 9, pp. 5807–5815, Sep. 2016.

[4] S. Yan, J. Chen, T. Yang, and S. Hui, "Improving the performance of direct power control using duty cycle optimization," *IEEE Trans. Power Electron.*, vol. 34, no. 9, pp. 9213–9223, Sep. 2019.

[5] T. Tao, W. Zhao, Y. Du, Y. Cheng, and J. Z. Jihong, "Simplified fault-tolerant model predictive control for a five-phase permanent-magnet motor with reduced computation burden," *IEEE Trans. Power Electron.*, to be published, doi: 10.1109/TPEL.2019.2934578.

[6] P. Cortés, M. P. Kazmierkowski, R. M. Kennel, D. E. Quevedo, and J. Rodríguez, "Predictive control in power electronics and drives," *IEEE Trans. Ind. Electron.*, vol. 55, no. 12, pp. 4312–4324, Jul./Aug. 2008.

[7] C. S. Lim, E. Levi, M. Jones, N. A. Rahim, and W. P. Hew, "FCS-MPC-based current control of a five-phase induction motor and its comparison with PI-PWM control," *IEEE Trans. Power Electron.*, vol. 61, no. 1, pp. 149–163, May 2014.

[8] P. Cortes, J. Rodriguez, D. E. Quevedo, and C. Silva, "Predictive current control strategy with imposed load current spectrum," *IEEE Trans. Power Electron.*, vol. 23, no. 2, pp. 612–618, Mar. 2008.

[9] P. Cortes, J. Rodríguez, C. Silva, and A. Flores, "Delay compensation in model predictive current control of a three-phase inverter," *IEEE Trans. Ind. Electron.*, vol. 59, no. 2, pp. 1323–1325, Jun. 2012.

[10] Q. Chen, W. Zhao, G. Liu, and Z. Lin, "Extension of virtual-signal-injection-based MTPA control for five-phase IPMSM into fault tolerant operation," *IEEE Trans. Ind. Electron.*, vol. 66, no. 2, pp. 944–955, Feb. 2019.

[11] M. Bermudez, I. Gonzalez-Prieto, F. Barrero, H. Guzman, M. J. Duran, and X. Kestelyn, "Open-phase fault-tolerant direct torque control technique for five-phase induction motor drives," *IEEE Trans. Ind. Electron.*, vol. 64, no. 2, pp. 902–911, Feb. 2017.

[12] X. Wang, Z. Wang, and Z. Xu, "A hybrid direct torque control scheme for dual three-phase PMSM drives with improved operation performance," *IEEE Trans. Power Electron.*, vol. 34, no. 2, pp. 1622–1634, Feb. 2019.

[13] Y. Wang *et al.*, "Deadbeat model-predictive torque control with discrete space-vector modulation for PMSM drives," *IEEE Trans. Ind. Electron.*, vol. 64, no. 5, pp. 3537–3547, May 2017.

[14] X. Wei *et al.*, "Finite-control-set model predictive torque control with a deadbeat solution for PMSM drives," *IEEE Trans. Ind. Electron.*, vol. 62, no. 9, pp. 5402–5410, Sep. 2015.

[15] Y. Zhang and J. Zhu, "A novel duty cycle control strategy to reduce both torque and flux ripples for DTC of permanent magnet synchronous motor drives with switching frequency reduction," *IEEE Trans. Power Electron.*, vol. 26, no. 10, pp. 3055–3067, Oct. 2011.

[16] Y. Zhang and H. Yang, "Model predictive torque control of induction motor drives with optimal duty cycle control," *IEEE Trans. Power Electron.*, vol. 29, no. 12, pp. 6593–6603, Dec. 2014.

[17] C. Xue, W. Song, and X. Feng, "Finite control-set model predictive current control of five-phase permanent-magnet synchronous machine based on virtual voltage vectors," *IET Elect. Power Appl.*, vol. 11, no. 5, pp. 836–846, May 2017.

[18] I. Gonzalez-Prieto, M. J. Duran, J. J. Aciego, C. Martin, and F. Barrero, "Model predictive control of six-phase induction motor drives using virtual voltage vectors," *IEEE Trans. Ind. Electron.*, vol. 65, no. 1, pp. 27–37, Jan. 2014.

[19] C. Xue, W. Song, X. Wu, and X. Feng, "A constant switching frequency finite-control-set predictive current control scheme of a five-phase inverter with duty-ratio optimization," *IEEE Trans. Power Electron.*, vol. 33, no. 4, pp. 3583–3594, May 2018.

[20] Y. Luo and C. Liu, "A simplified model predictive control for a dual three-phase PMSM with reduced harmonic currents," *IEEE Trans. Power Electron.*, vol. 65, no. 11, pp. 9079–9089, Nov. 2018.

[21] G. Li, J. Hu, Y. Li, and J. Zhu, "An improved model predictive direct torque control strategy for reducing harmonic currents and torque ripples of five-phase permanent magnet synchronous motors," *IEEE Trans. Ind. Electron.*, vol. 66, no. 8, pp. 5820–5829, Aug. 2019.

[22] C. Xiong, H. Xu, T. Guan, and P. Zhou, "A constant switching frequency multiple-vector-based model predictive current control of five-phase PMSM with nonsinusoidal back EMF," *IEEE Trans. Ind. Electron.*, vol. 67, no. 3, pp. 1965–1707, Mar. 2020.

[23] Z. Zhou, C. Xia, Y. Yan, Z. Wang, and T. Shi, "Torque ripple minimization of predictive torque control for PMSM with extended control set," *IEEE Trans. Ind. Electron.*, vol. 64, no. 9, pp. 6930–6939, Sep. 2017.

[24] L. Tarisciotti, P. Zanchetta, A. Watson, J. C. Clare, M. Degano, and S. Bifaretti, "Modulated model predictive control for a three-phase active rectifier," *IEEE Trans. Ind. Appl.*, vol. 51, no. 2, pp. 1610–1620, Mar./Apr. 2015.

[25] D. Zhou, P. Tu, and Y. Tang, "Multivector model predictive power control of three-phase rectifiers with reduced power ripples under nonideal grid conditions," *IEEE Trans. Ind. Electron.*, vol. 65, no. 9, pp. 6850–6859, Sep. 2018.

[26] Z. Zhang, H. Fang, F. Gao, J. Rodríguez, and R. Kennel, "Multiple-vector model predictive power control for grid-tied wind turbine system with enhanced steady-state control performance," *IEEE Trans. Ind. Electron.*, vol. 64, no. 8, pp. 6287–6298, Aug. 2017.

[27] Y. Zhang and H. Yang, "Generalized two-vector-based model-predictive torque control of induction motor drives," *IEEE Trans. Power Electron.*, vol. 30, no. 7, pp. 3818–3829, Jul. 2015.

Wenxiang Zhao (M'08–SM'14) received the B.Sc. and M.Sc. degrees from Jiangsu University, Zhenjiang, China, in 1999 and 2003, respectively, and the Ph.D. degree from Southeast University, Nanjing, China, in 2010, all in electrical engineering.

Since 2003, he has been with Jiangsu University, where he is currently a Professor with the School of Electrical Information Engineering. From 2008 to 2009, he was a Research Assistant with the Department of Electrical and Electronic Engineering, University of Hong Kong, Hong Kong. From 2013 to 2014, he was a Visiting Professor with the Department of Electronic and Electrical Engineering, University of Sheffield, Sheffield, U.K. His current research interests include electric machine design, modeling, fault analysis, and intelligent control. He has authored and coauthored more than 200 technical papers in these areas.

Tao Tao received the B.Sc. degree in electrical engineering from Nanjing Agricultural University, Nanjing, China, in 2009. He is currently working toward the Ph.D. degree in electrical engineering with Jiangsu University, Zhenjiang, China.

His research interests include control of multiphase permanent-magnet machines.

Jihong Zhu received the B.Sc. degree in electrical engineering from Jiangsu University, Zhenjiang, China, in 1990, and the Ph.D. degree in control engineering from Nanjing University of Science and Technology, Nanjing, China, in 1995.

From 1996 to 1997, he was with Nanjing University of Aeronautics and Astronautics, Nanjing, China, where he was a Postdoctor and an Associate Professor, respectively. Since 1998, he has been with Tsinghua University, where he is currently a Professor. His teaching and research interests include motor control and flight control. He has authored or coauthored more than 150 technical papers, and is the holder of more than 60 patents in these areas.

Huajun Tan received the B.Sc. degree in electrical engineering from Jiangsu University, Zhenjiang, China, in 2018. He is currently working toward the M.Sc. degree in electrical engineering in Jiangsu University, Zhenjiang, China.

His research interests include servo motor control system.

Yuxuan Du received the B.Sc. degree in electrical engineering in 2017 from Jiangsu University, Zhenjiang, China, where he is currently working toward the Ph.D. degree in electrical engineering.

His research interests include power electronics and permanent-magnet motor control.